Molecular dynamics simulations of CNTs and CNT-nanocomposite under ballistic impact

Submitted By:

Komal Rathi

Enrollment No. 2015PDE5197

Project Guide:

Dr. Dinesh Kumar

A Thesis Submitted in Partial Fulfillment of the Requirements for the Award of the Degree of

Master of Technology

in

Design Engineering

Department of Mechanical Engineering

Malaviya National Institute of Technology

June 2017

CANDIDATE'S DECLARATION

I hereby declare that the work presented in this dissertation entitled, **"Molecular dynamics simulations of CNTs and CNT-nanocomposite under ballistic impact"** in partial fulfillment for the award of degree of **"Master of Technology"** in Mechanical Engineering with specialization in Design Engineering and submitted to the Department of Mechanical Engineering, Malaviya National Institute of Technology is a record of my own investigation carried under the supervision of Dr. Dinesh Kumar, Assistant Professor, Department of Mechanical Engineering, Malaviya National Institute of Technology. I have not submitted the matter presented in this dissertation anywhere else for the award of any other degree.

Date: KOMAL RATHI
Place: MNIT, Jaipur 2015PDE5197

CERTIFICATE

This is to certify that the project report entitled **"Molecular dynamics simulations of CNTs and CNT-nanocomposite under ballistic impact"** submitted by KOMAL RATHI, ID. No. 2015PDE5197 is an authentic work carried out by her at Malaviya National Institute of Technology, Jaipur under my guidance. The matter embodied in this project work has not been submitted earlier for the award of any degree to the best of my knowledge and belief.

Date:

Dr. Dinesh Kumar
Assistant Professor
Department of Mechanical Engineering
Malaviya National Institute of Technology, Jaipur

Acknowledgement

This thesis I present here would not have been possible without the support of several person whom I would like to thank.

First of all, I would like to thank my thesis advisor Dr. Dinesh Kumar for his patience and abundance of encouragements. I am grateful for his support and for him giving me the freedom to explore many opportunities and the guidance when I needed. My special thanks to PhD scholar Mr. Akhileshwar Singh for his consistent support and suggestions. I am also grateful to the MNIT for providing all the facilities at Material Research Centre required to carry out my thesis work.

Furthermore, I owe thanks to my friends for their time to listen, for their support, encouragement and valuable discussions during my thesis.

Finally, most importantly, I am indebted to my family for all the encouragement and moral support all the time. I am highly thankful to the one due to whom I am here today. It has been a long journey up until finishing the thesis.

KOMAL RATHI

Abstract

The main aim of this thesis is to calculate the maximum energy absorbed by CNT and CNT-nanocomposite under blast impacts. This study is based on Molecular Dynamics (MD) simulations. While analyzing CNT, two main types of defects have been considered, namely vacancy defect and Stone Wales (SW) defect. Modeling of defects has been done using Virtual Nanolab 2016.3 (VNL), and Material Studio 8.0 is used for modeling and optimization of polymer (Epon-862) -CNT nanocomposite. LAMMPS scripts were written to carry out various simulations on CNTs and CNT-nanocomposite. Tersoff-Brenner and PCFF potential define the interatomic interactions of the CNT and the nanocomposite, respectively. Results of simulations have been visualized using OVITO 2.7.1 (Open Visualization Tool). A bullet made up of diamond is struck on the CNT and nanocomposite to carry out ballistic impact and the maximum energy absorbed by them is calculated. It is found that maximum energy absorbed by a defective CNT is less than the pristine CNT, and that the amount of energy absorbed decreases as the number of defects in CNT increases. It is further concluded that if CNTs are reinforced in to a polymer matrix, the amount of energy absorbed by the resulting nanocomposite is increased many folds. Thus, CNT-nanocomposites are found to be quite promising for making armors for blast mitigation.

Contents

List of Figures

List of Symbols

Symbols	**Description**
Ch	Chiral Vector
θ	Chiral Angle
â1, â2	Unit Chiral Vector
V_{bl}	Ballistic Limit
A_p	Areal Density
E_s	Specific Ballistic Energy
M	Mass of bullet
ρ_i	Density of *i*th layer of fabric
t_i	Thickness of *i*th layer of fabric
V_i	Initial Velocity of projectile
V_r	Final Velocity of projectile
F_i	Force acting on ith atom
U	Potential Energy of the system
r_i	Position vector of ith atom
K	Kinetic Energy of the system
$F_i(\rho_i)$	Embedding Energy Function
r_{ij}	Scalar distance between ith and jth atom

Chapter-1

INTRODUCTION

1.1 Discovery of CNTs

Carbon nanotubes (CNTs) are made by rolling seamless graphene sheets and have extraordinary mechanical properties. C60 molecule was discovered by Harry Kroto in 1985[1], during the experimentation of vaporization of graphite using laser beams by laser ablation system. The graphite vapors were deposited on copper plates. During 1990s arc discharge method was used to make C60 molecule in bulk. In 1991, Iijima used this technique to vaporize fullerenes by supplying large current between graphite rods and deposit them on copper tip. When the results were observed through an electron microscope, carbon nanotubes were deposited at the negative electrode [2]. Tiny pure carbon tubes along with other forms of carbons were obtained. The first CNTs were multi-walled with concentric layers having caps at the ends.

1.2 Types of Carbon Nanotube

Two types of carbon nanotubes based on number of graphene layers are as follows-

1.) Single Wall Carbon Nanotubes (SWNTs)- Single layer of graphene.

2.) Multi Wall Carbon Nanotube (MWNTs)- More than one layers of graphene.

The properties of both are different because of difference in their structural compositions.

1.2.1 Single-walled carbon nanotube (SWCNT)

A single sheet of graphene rolled up in the form of cylinder is Single-walled CNT. Lengths of SWNTs are extended to microns and diameters are usually in the range of 0.4-1.0 nm. SWNTs have axial symmetry which justifies its unique properties [3]. But this symmetry can be considered only if we ignore two end-caps present in SWNTs. Fig. 1.1 depicts the shape of SWNT.

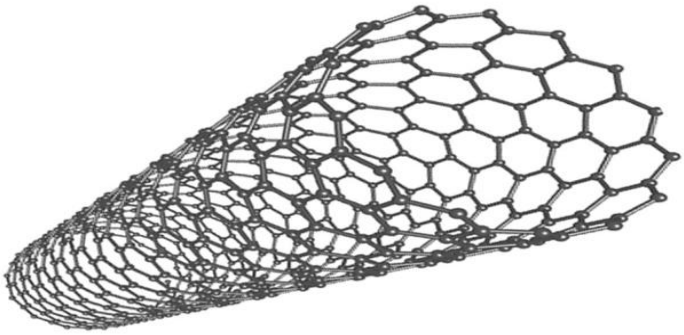

Fig 1.1 SWNT.

1.2.2 Multi-Walled Carbon Nanotube (MWNT)

Another type of CNT is multi-walled carbon nanotube. It is called so because of multiple concentric layers of graphene arranged coaxially around central axis. The spacing of inter layer is around .34 nm [4]. It has greater diameter as compared to SWNTs. Also, MWNTs are stronger than SWNTs. Figure 1.2 depicts MWCNT with 0.34 nm spacing.

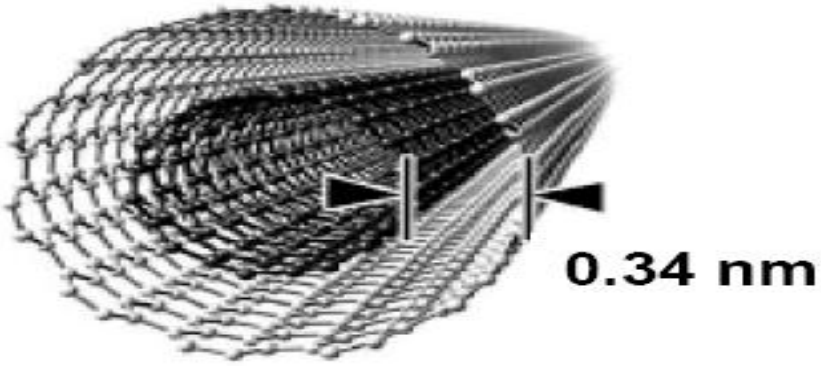

Fig. 1.2 MWCNT.

Usually MWNTs have diameters in the range 2.5 - 100 nm having 2 to 30 layers of graphene sheets.

1.3 Classification of Carbon Nanotubes

Single walled carbon nanotubes have different configurations. These configurations are dependent on orientation of hexagon (six-member) ring of carbon relative to the axis of the nanotube in the honeycomb lattice. The three configurations of SWNT are-

1.) Armchair carbon nanotube,

2.) Zigzag carbon nanotube, and

3.) Chiral carbon nanotube.

Fig. 1.3 depicts configurations of each of three nanotubes. CNTs have many chiralities because in graphite lattice six-member ring can be oriented in any arbitrarily direction with respect to the axis of nanotube. While calculating chirality, only distortion of curvature of nanotubes is considered while distortion of the hexagons is neglected.

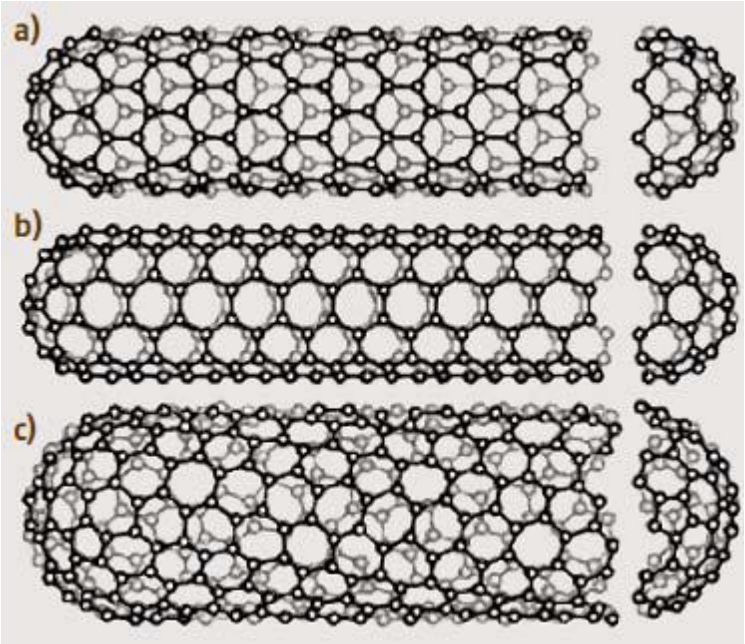

Fig. 1.3 Formation of CNTs: a) Zigzag CNT, b) Arm-chair CNT, and c) Chiral CNTs **.**

1.4 Carbon nanotubes on the Basis of Chirality

On the basis of chirality, CNTs are categorized as:

a) Armchair and zigzag nanotubes, and

b) Chiral nanotubes.

A carbon nanotube is said to be achiral if its mirror image is identical and carbon nanotubes are chiral if its mirror image has spiral symmetry i.e., mirror image can't be superimposed. Achiral nanotube is either zigzag or armchair [4].

Each carbon nanotube structure has chiral angle (θ), and a chiral vector C_h defined below [5]:

$$C_h = n\hat{a}_1 + m\hat{a}_2 \quad (1.1)$$

While the integers n and m are the number of steps along the unit chiral vectors represents vectors, $\hat{a}_1$ and $\hat{a}_2$ respectively, as shown in Fig. 1.4.

The chiral angle (θ) determines the amount of twist of CNTs, where values of θ are in the range of $0 \leq \theta \leq 30$ [6]. Chiral angle is depicted in Fig. 1.4.

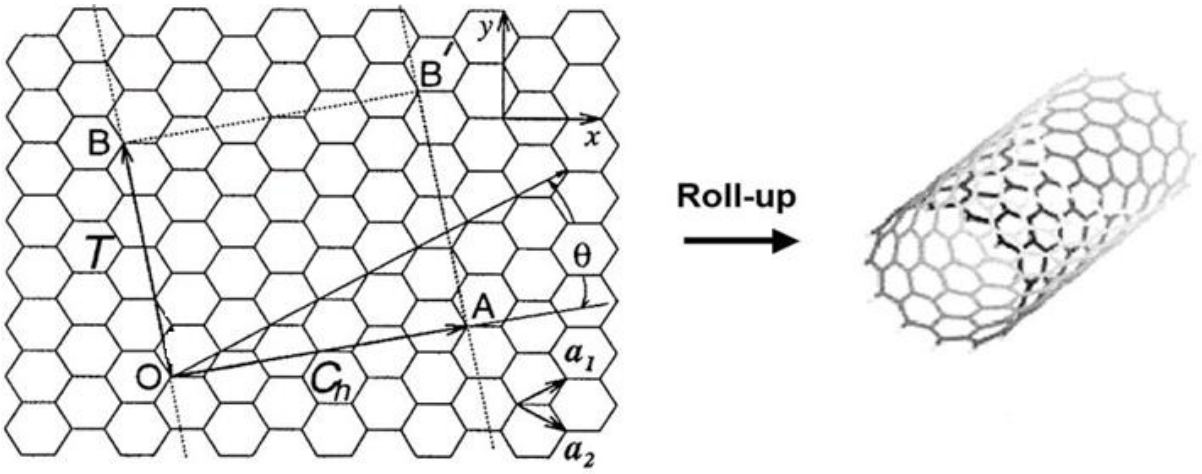

Fig. 1.4 Graphene rolled up into a tube [4].

Where, if n = m and $\theta=0^0$ then it represents armchair CNT, m = 0 and $\theta=30^0$ then it represents zigzag type CNT, and when $n \neq m$ and $0^0 < \theta < 30^0$, it represents chiral type CNT. Fig. 1.5 shows the schematic configuration of three types of CNTs discussed above [7].

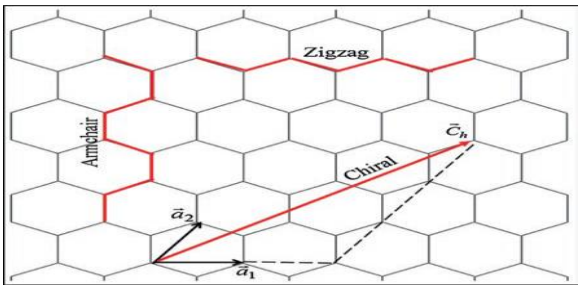

Fig. 1.5 Schematic view of single-walled zigzag, armchair and chiral nanotube.

1.5 Properties of carbon nanotube

The properties of carbon nanotubes such as thermal, electrical, magnetic, conductivity, lattice energy and density are dependent on structure of the nanotube. For instance, the properties of nanotubes are highly influenced by the variation in diameter, e.g., the tube with larger diameter will show properties similar to graphite and the narrower diameter CNT shows intrinsic properties.

1.5.1 Mechanical Properties

Carbon nanotube has very high tensile strength and elastic modulus. Its high strength is attributed to sp^2 covalent bonds. In 2000, a study showed that multi-walled carbon nanotube had a tensile strength of 63 GPa. Later in 2008, another study stated that the strength was up to 100 GPa (15,000,000 psi), which satisfied quantum/atomistic models. Carbon nanotubes have a low density and very high specific strength. The specific strength of CNT is best in any known material. Even high-carbon steel has lower maximum specific strength than CNT i.e., 154 KN.m/kg. CNT doesn't perform well under compression. They have high aspect ratio and hollow structure due to which they undergo buckling under torsional, compressive or bending stress.

In 1997, a study stated that the value of Young's Modulus of CNTs lies in the range between 0.97 to 1.11 TPa on the basis of empirical force constant model. In 1999, the value was reported to be approximately 1.25 TPa. More recent experimental observations using Atomic Force Microscopy (AFM) resulted in Young's Modulus value = 1.2 TPa, which is very high.

1.5.2 Electrical properties

Chirality of an CNT can also define its electrical property. If (n - m) and (2n + m) are a multiple of 3, the CNT is said to be metallic, otherwise it is semiconducting. If n is a multiple of 3, an armchair nanotube (having m = n) would always be metallic, and the same is true in the case of zigzag nanotubes because value of m is 0. In Fig. 1.6, the encircled dots correspond to metallic CNTs and the small dots represents semiconducting CNTs. Metallic CNTs carry 4×10^9 A/cm^2 electric current density, which is 1,000 times more as compared to metals like copper. Also, copper has limited current density because of electro-migration. This effect is not applicable for carbon nanotubes.

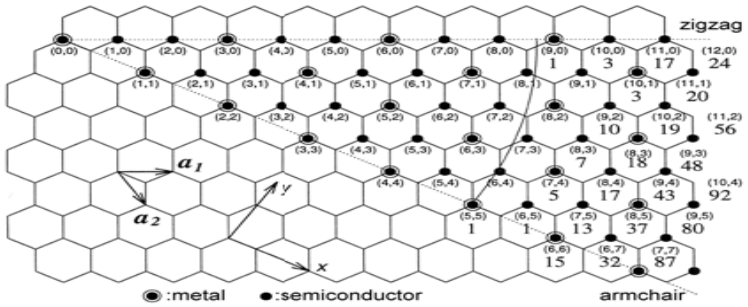

Fig. 1.6 Possible values of integers m and n for metallic CNTs, and semiconducting CNTs.

1.5.3 Optical Properties

CNTs exhibit an exceptionally high third-order optical nonlinearity and nonlinear saturable absorption with ultrafast recovery time and broad bandwidth operation. Thus, they are becoming key components towards the development of fiber lasers, nonlinear photonic devices and several emerging next generation devices.

1.5.4 Thermal properties

The heat flow and thermal conductivity along main axes in CNTs is estimated to be about 3500 $Wm^{-1}K^{-1}$, which is higher than diamond having thermal conductivity in the range of 900-2300 $Wm^{-1}K^{-1}$. The thermal conductivity is specifically more along the main axis of CNTs, due to the easy propagation of atomic vibrations along the tube. In the direction transverse to its axis, however, the nanotube is much less rigid and the thermal conductivity in that direction is about a factor of 100 lesser.

1.6 Defect in CNTs

Defects are commonly found in all the materials and it affects their properties. The most prevalent defects in CNTs are discussed as follows-

1.6.1 Atom Vacancy

Vacancy defect is said to occur when one or more atoms in CNTs are absent. This defect occurs naturally in hexagonal lattice. Fig. 1.7 depicts CNT in which one carbon atom is missing. Such defect is known as monovacancy.

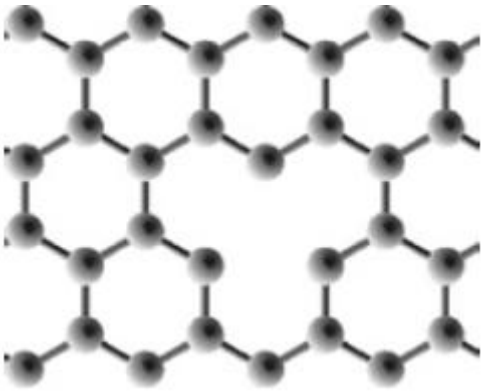

Fig. 1.7 CNT with monovacancy.

1.6.2 Stone-Wales defect

When the four adjacent hexagon rings transform into 5-7-7-5 configuration or a pair of heptagons-pentagons, the defect is known as Stone-Wales defect. The defect influences electrical, mechanical and thermal properties to different extent. Fig. 1.8 depict CNT with single SW defect.

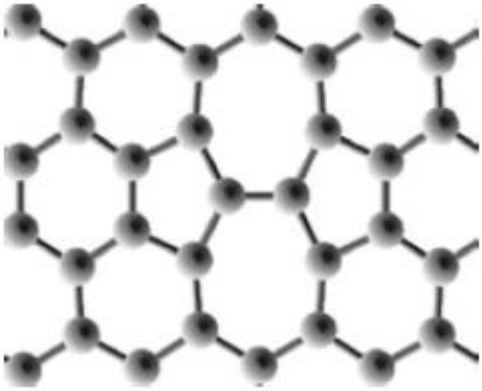

Fig. 1.8 CNT with Stone-Wales defect.

1.6.3 Kink Junctions

Two CNTs of different chiralities form intramolecular connections in such a way that strain energy is minimized and knee connection is made to cover the chirality gap. These are generally used to produce molecular-size metal-metal, metal-semiconductor or semiconductor-semiconductor nanojunctions in carbon nanoelectronics. Fig. 1.9 depicts kink junction between two CNTs.

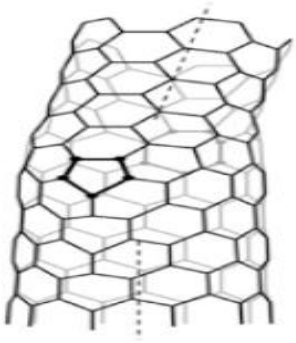

Fig. 1.9 Knee Junction between CNTs of different diameters.

1.6.4 Welded CNTs

Two CNTs are welded together at elevated temperatures to form stable geometries like X, Y and T. These CNTs can be used as multi terminal electronic devices. Fig. 1.10 depicts welded CNTs.

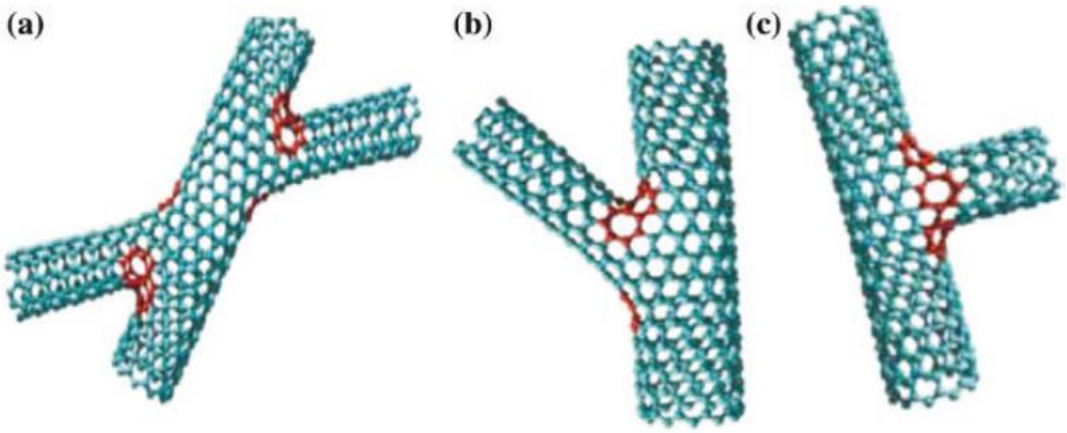

Fig. 1.10 Welded CNT with- a) X-geometry, b) Y-geometry, and c) T-geometry.

1.6.5 Substitutional doping defect

To modify the electrical, vibrational, chemical and mechanical properties of CNTs, carbon atoms are replaced by non-carbon atoms. Most commonly doped atoms are nitrogen, silicon and boron. Fig. 1.11 depicts Si doping in single-walled CNT.

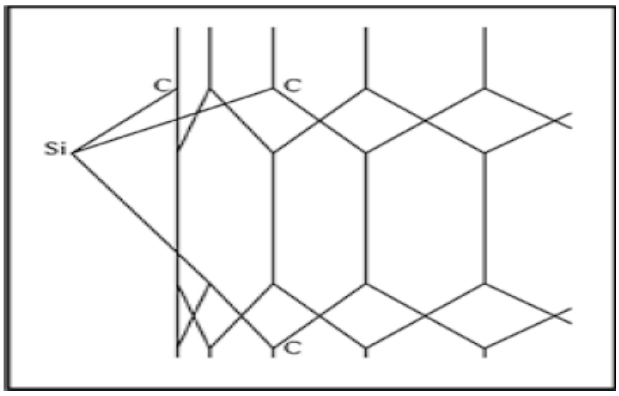

Fig. 1.11 Si doping in SWNT.

1.6.6 Perturbation

The atoms of hexagons in CNTs are misplaced in experimental studies because of the local stresses and the effect of environmental pressure. This defect also influences the mechanical properties of CNTs. Fig. 1.12 depicts perfect and perturbated CNTs.

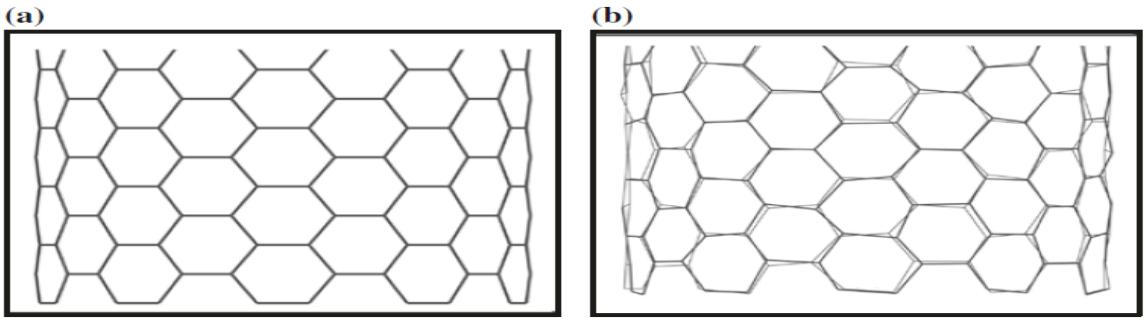

Fig. 1.12 a) perfect CNT and b) 10% perturbated CNT.

1.7 Introduction to Composites

Composites are made of two or more components combined together to achieve some exceptional mechanical, chemical and physical properties. Composites offer higher stiffness, lower weight, more strength, lower expansion coefficient, easy manufacturing of complex shapes and better corrosion resistance. Composites can be classified into three different types-

I. Particle reinforced- dispersion strengthened and large particle composites.
II. Fiber reinforced- long fiber and -short fiber composites.
III. Structural- sandwich panels and laminates.

1.7.1 CNT Based Composites

If one of the constituent phases in composites is less than 100 nm in size, the composite is known as nanocomposite. In today's world of advanced technologies, monolithic material and their alloys do not meet the expectations to fulfill the requirements of new technologies. Composites material have better properties and wider applications as compared to monolithic materials. By reinforcing the ceramic, metallic or polymeric matrix with CNTs better mechanical strength, higher significant temperature and more chemical durability can be achieved. These combinations have improved physical and chemical properties. As discussed earlier, CNT has exceptionally good properties, it can prove to be very promising reinforcement and enhance the properties as per the requirements.

1.8 Ballistic Energy Absorption

When a bullet with certain velocity strikes an armor, it passes through multiple fibers which absorbs the kinetic energy transferred by it. The stress waves carry kinetic energy which is dissipated in deformation of fibers and the friction between fibers during sliding. The performance of armor is highly influenced by the frictional characteristics and structure of fiber. The consecutive layer of fiber absorb the energy which was left undissipated until the bullet was stopped. In multilayer fabric, energy absorption is usually increased as the stress waves travel in transverse as well as planar directions.

1.8.1 Ballistic Fibers performance measures

Two main characterizing factors of ballistic performance of a fabric are its specific ballistic energy (used to represent the mass efficiency) and ballistic limit.

The ballistic limit V_{bl}(m/s) is defined as the velocity, at which bullet of mass m (kg) with A_p (kg/m^2) as its areal density, just starts to penetrate the armor.

The specific ballistic energy (J.m^2/kg) is kinetic energy at ballistic limit and can be written as Eq. 1.2 [8]-

$$E_s = \frac{mV_{bl}^2}{2A_p} \tag{1.2}$$

where, $A_p = \sum_{i=1}^{n} \rho_i \, t_i$; (1.3)

ρ_i= density of *i*th layer, t_i= thickness of *i*th layer.

The dissipated kinetic energy of projectile is given by Eq. 1.4 [8]-

$$E = \frac{1}{2} m(V_i^2 - V_r^2) \tag{1.4}$$

where,

E= energy dissipated (J),

V_i =Initial velocity of projectile (m/s),

V_r= Residual projectile velocity after penetration (m/s)

If , V_r=0 i.e., there is no penetration of bullet or partial penetration, the equation of dissipated energy reduces to Eq. 1.5 [8].

$$E = \frac{1}{2}m(V_i^2) \quad (1.5)$$

1.9 Objective of the Thesis

Safety in defense is one of the major concerns now-a-days. Various materials for armor design are available in market. The main focus of this study is to observe the behavior of defective CNTs and nanocomposite under ballistic impact. Molecular Dynamics(MD) simulations are used to make the calculations more efficient and reduce the computational cost. Maximum energy absorded by CNTs with both end fixed have been evaluated. Defects have been induced in CNTs to study the variations in energy absorbed. Tersoff-Brenner potential has been used for CNTs to observe their deformation phenomenon. Epon-862 polymer is reinforced with CNTs to make a nanocomposite and the results have been evaluated. PCFF potential is used in the case of nanocomposite. Bullet is struck at different heights of CNT with varying speed to find the conditions required to attain maximum energy absorption.

Chapter-2

Literature Survey

2.1 Literature Review

CNTs have high stiffness [9] , superior thermal [10], optical [11] and electrical properties [12] due to which they are ideal for reinforcement of composites. According to Krishnan et al. [13], the average value of Young's modulus of carbon nanotubes in the diameter range 1.0-1.5nm, is very high, i.e., about 1.25 (-0.35/+0.45) TPa**.** CNT fibers were examined and their Young's Modulus and tensile strength were more than the twice of corresponding steel wires and were around 20 times as tough [14]. Jin and Yuan [15] evaluated mechanical properties of SWNT by using numerical simulations by using both energy and force approaches and reported the values of shear modulus to be 0.546 and 0.492 TPa, respectively. In a Molecular Dynamics (MD) study by Mylvaganam and Zhang [16] the potential application of CNTs as blast resisting materials was examined and the energy absorbing capacity of CNT was found to be quite high. In this study, CNTs with different chiralities and boundary conditions subjected to bullet impact were discussed for absorbed energy. The test was conducted over a range of bullet speeds that a CNT could sustain without failure. The bullet was made of diamond with dimensions $35.67\times35.67\times7.13\ \mathring{A}^3$ and assumed to have a flat tip. The interactions between carbon atoms of CNT were defined by three body Tersoff-Brenner potential. The impact was for short time period, hence energy loss was neglected during the simulation. It was observed that CNTs with greater radii absorbed more energy. However, definite relation between variation of absorbed energy with radii could not be established. A linear relationship between CNT length and absorbed energy was established in this study. In another study, the author also presented case study on use of CNTs as armor systems. It was suggested that multiple layer of CNT fibers was required for efficient CNT armor system [17]. However, it is almost impossible to have CNTs without defects [18]. CNTs can have many type of defects such as vacancy defects, heptagons, pentagons, heterogeneous atoms, discontinuities and distortions. The main reasons for defects in CNTs are large buckling forces on the tubes [19], high energy discharge such as arc or laser discharge [20], kinetic force for formation of CNTs and impurities present in catalyst during precipitation or diffusion in CVD process [21]. Due to these defects, carbon layer in CNT loses

its symmetry and its mechanical properties are affected severely and reduces their application [22].

Many options are available for armor materials such as ceramic armors (silicon carbide), laminated armors (Aluminium foam), flexible composite armors (Kevlar, Twaron and Spectra fibers based) and nanocomposite (CNT and graphene based) armors [8]**.** Brittle polymers, such as polystyrene, poly(methyl methacrylate) and epoxies, alone can't be used for bullet proof vests as they will break as soon as the bullet strikes them, therefore toughening these polymer by halloysite nanotube may their increase impact resistance, as concluded by Ye et al. [23]. Polymer-based composite materials are being widely used in marine, military, automotive industry and aerospace, because of their high strength, great stiffness and low density. Initially fiber metal laminate panels were used but they had low interlaminar fracture toughness properties which lead to their failure [24]. Epoxy is sometimes used as matrix materials in the composites**.** Impact damage resistance of CFRP with nanoclay- filled epoxy matrix was studied by Iqbal et al. [25], results showed that both damage resistance and damage tolerance were improved, but they failed due to delamination. Taha et al. [26] observed that addition of 2% to 4% CNTs by weight to epoxy interfaces results in enhancement of the composite ability to resist blast. The effect of simultaneous presence of MWNT's and nanoclays on the mechanical properties was studied by Ayatollahi [27] and it was established that Young's Modulus and fracture toughness were improved but there was reduction in ultimate tensile strength. Carbon filled polymer composites have relatively high specific mechanical properties [28]. The addition of 0.5% of MWCNTs to woven Kevlar/epoxy laminated composite resulted in about 35% increase in energy absorption properties at ambient temperature, and the addition of 0.3% of MWCNTs increase the energy absorbing capability by 34% at low temperature [29]**.** Carbon nanotubes have high potential in enhancing the electrical, thermal and mechanical properties of the polymers [30]. By using CNTs with brittle materials like epoxy, Young's Modulus of the resulting composites can be enhanced, thus making them one of the best reinforcements for polymers [31]. Moreover, the mechanical properties of epoxy are said to be higher than that of other blast resisting materials like polyurea and polyurethane [32]. The application of CNT-polymer composites for blast impact was studied by Grujicic et al. [33]. E-glass continuous fiber was used as reinforcement in poly-vinyl-ester-epoxy matrix (PVEE) matrix in making the armor. MWNT reinforced PVEE mats were used to interlace composite matrix laminas. The study

showed that the performance under blast of hybrid armor system is affected by the thickness and location of PVEE mats reinforced with MWCNT. The laminate with total thickness of 12.7 mm was taken. The 0.30 caliber fragment with 610 m/s speed of penetration simulated for the ballistic test. The difference in acoustic impedance of 100% E-glass/epoxy lamina and PVEE-MWCNT mat varies between 5% to 6%. A double-layered PVEE-MWCNT mat with thickness around 100 μm was observed to absorb more energy because more energy was required to penetrate the thicker mat.

2.2 Research Gap

Body armor has been evolved over thousands of years of improvement with the help of advances in material science. CNT and CNT-based hybrid polymer composites are very effective for ballistic armors as they have several functional benefits. The enhanced mechanical properties of CNT based nanocomposites have drawn interest of many researchers [8]. Some of the important factors to be considered are viability in the manufacturing aspects and cost effectiveness.. Though, still at very initial stage in development, simulations and experiments have demonstrated the potentiality of CNTs and CNT nanocomposites as body armor materials that possess superior anti-ballistic properties. More research still needs to be conducted to verify and validate a few hypothetical claims and ideas related to ballistic resistant capability and functions of CNT and CNT nanocomposites.

Chapter-3

Introduction to Molecular dynamics

3.1 Introduction

Molecular dynamics (MD) is a simulation method, which integrates Newton's equation of motion to study the evolution of a set of interacting atoms and molecules of a system. The motion of interacting atoms and molecules is observed for a fixed interval of time. The trajectories of the particles are obtained by solving Newton's equations of motion and force fields are used to define potential energy and force between particles. MD simulation has its applications in material science and is quite useful for studying biomolecules and proteins. In 1957, the concept of classical molecular dynamics method was introduced for the first time and that study include molecular interactions of 500 hard spheres. Moreover, the motion of 864 individual atoms of liquid argon was studied. To increase the calculation speed and divide the load between processors parallel computing is used. The major task of CPU (Central Processing Unit) is evaluation of force field (potential) as a function of the coordinates of atoms in a classical MD simulation. The non-covalent or non-bonded part is the most time consuming in evaluating the force field. The integration time step is also an important factor which influences the time taken by the CPU for simulation. Time step is defined as time between evaluations of the force field. It must be small enough to avoid discretization errors (must be small than the fastest vibration frequency of the system). Classical MD typically uses the time step of order of 1 femto second (10^{-15}).

3.2 Interatomic potential

In classical molecular dynamics, there is interaction between atoms. Due to these interactions forces are applied on atoms causing their movement. The movement of atoms changes the forces on them as well as relative positions. Forces acting on atoms are dependent on the particle/atom coordinates and defined as gradient of the potential energy function.

$$F_i = -\frac{\partial U}{\partial r_i} \qquad (3.1)$$

Here, r_i is the position vector of *i*th atom. *U* denotes the potential energy of the system which is a function of the positions of the atoms. There is no change in function with rotation or translation of configuration of atom i.e., function is invariant. It does not depend on the absolute positions. The function varies with relative positions. Eq. 3.1 represents law of conservation of mechanical energy $E = K+U$ applied to the atoms. Here, K represents kinetic energy.

3.3 Potentials in MD simulations

3.3.1 Embedded atom method (EAM)

This is an approximation method used to describe the energy between atoms. Electron density is one of the major factors in calculating energy. The energy is dependent on both pair potentials and embedding energy. Daw and Baskes (1984) developed this potential to study the defective metals. EAMs have wide application in MD simulations because of their simplicity. Eq. 3.2 represents the mathematical form of EAM :

$$U_{EAM} = \sum_i F_i(\rho_i) + \sum_{i \neq j} U_{ij}(r_{ij}) \quad (3.2)$$

where, $F_i(\rho_i)$= Embedding energy function

r_{ij}= Scalar distance between *i*th and *j*th atoms

Second summation represents pair interactions without double counting (Eq. 3.3)-

$$\frac{1}{2}\sum_{i \neq j}^{N} U_{ij}(r_{ij}) = U_{12} + U_{13} + \ldots + U_{23} + U_{24} + \ldots U_{34} + U_{35} + \ldots + U_{45} + U_{46} \quad (3.3)$$

The electron density is represented by linearly superimposing the valence clouds from other atoms-

$$\rho_i = \frac{1}{2}\sum_{j(\neq i)} \rho_j(r_{ij}) \quad (3.4)$$

3.3.2 Empirical Potentials

In chemistry potentials are frequently called force fields, while in material physics these are called just analytical or empirical potentials. Most commonly used force fields in chemistry is empirical. These are the summation of bonded forces related to bond angles, chemical bonds, bond dihedrals and torsional forces and non-bonded forces related to electrostatic charge van der Waals forces. The total potential energy is given by:

$$E_{pot} = \Sigma V_{bond} + \Sigma V_{ang} + \Sigma V_{torsion} + \Sigma V_{vdw} + \Sigma V_{ele} + \dots \quad (3.5)$$

Its calculation is the major drawback as it reduces the speed of simulations. For example, Brenner potential for hydrocarbons and its extensions for the C-Si-H and C-O-H systems.

3.3.3 Pair wise Potentials & Many-body Potentials

In pair wise potential, only interaction between a pair of atoms is considered for calculating total potential energy. Leonard Jones potential which is used to calculate the van der Waals forces is an example of pair wise potential

While calculating total energy in many-body potential, effect of at least three particles or more than that interacting with each other is considered. In pair wise potential simulation, global interactions are present, but these are applicable only for pair wise terms. In many body potential calculation of energy is not same as that of pair wise potentials, as higher order terms are considered and calculations are done explicitly. For example, Tersoff potential is generally used for simulation of germanium, carbon and silicon.

3.3.4 Semi-Empirical Potentials

When a semi-empirical approach is applied to represent the interatomic potentials among a wide variety of elements and their alloys using a common mathematical formulation, the potential is known as semi-empirical potential. This type of potential is generally used to reproduce the fundamental, physical properties of a metal or its alloys.

3.3.5 Polarizable Potentials

It includes the effect of polarizability, e.g. by measuring the partial charges obtained from quantum chemical calculations. This allows for a dynamic redistribution of charge between

atoms which responds to the local chemical environment. For systems like water and protein better simulation results obtained by introducing polarizability.

3.4 Simulation Method in Molecular Dynamics

MD simulation is used for computing the transport and equilibrium properties of a many-body system. Laws of classical mechanics are applicable on classical molecular dynamics. The evolution of particles is determined from the initial set of velocities and positions of atoms (phase space). The trajectory thus obtained specifies the variation of velocities and position of the atoms in a system.

The solution of differential equation gives the trajectory.

The motion of particles can be described by following equation-

$$\frac{\partial^2 x}{\partial t^2} = \frac{F_{x_i}}{m_i} \tag{3.6}$$

where, $m_i =$ mass of i^{th} particle,

F_{x_i}= Net force on particle along the direction (x_i).

3.5 Steps Involved in Molecular Dynamics simulation

i. Assign the initial velocities and positions of the atoms

ii. Calculate the forces on all the atoms on the basis of interatomic potential and integrate Newton's equation of motion to obtain the trajectory.

iii. The above steps are core of the simulation. These steps are repeated to obtain time evolution of the desired property of the system.

3.6 Ensembles

3.6.1 NVE or Micro-canonical

In the micro-canonical ensemble NVE, atoms (N), volume of the system (V) and energy (E) are kept constant. They are independent variables. NVE ensemble updates velocity and positions for atoms at every timestep. It is similar to an adiabatic process without heat exchange. The

trajectory of atoms in the system is generated during which there is an exchange of potential and kinetic energy, and the total energy is conserved.

3.6.2 NVT or Canonical

In the canonical (NVT) ensemble, atoms (N), volume (V) and temperature of the system (T) are kept constant. Noose-Hover thermostat controls the temperature.

3.6.3 Isothermal–Isobaric or NPT

NPT is the isobaric-isothermal ensemble in which number of atoms (N), pressure (P) and temperature (T) are conserved. The volume of system changes over time. Nose-Hoover barostat and Nose Hoover thermostat control the emperature and pressure.

Chapter-4

Atomistic Models of CNTs and Nanocomposite

The software used for modeling and simulation are described below-

4.1 Virtual Nanolab (VNL)

VNL is one of the molecular dynamics software suitable for modeling and simulating the atomistic models. In the present study, Crystal Builder tool of VNL has been used for modeling of defective CNTs. Additional tools like tube wrapper were installed. This tool of VNL creates the crystal structure easily and one can also optimize the structure modeled by VNL, and LAMMPS data file can also be easily exported for further simulation.

4.2 BIOVIA Material Studio Amorphous Cell

BIOVIA Material Studio is a modeling and simulation module of Material Studio which helps researchers in chemistry and material science to understand atomic and molecular structure of materials. BIOVIA Material Studio Amorphous Cell was used for the modeling of nanocomposite. It is an extensive tool for building models of a variety of amorphous materials. It provides flexibility in choosing the force fields. Various construction options enables the modeling of bulk structure of variety of systems including glasses and polymers along with nanostructures. Layered structures which are useful for the study of interfaces can also be constructed using BIOVIA Material Studio Amorphous Cell.

Molecules grow in a three dimensional box by considering the interactions with the atoms already present and monitoring the conformations of single chain. All the structures undergo a variety of checks such as close contacts and ring spearing. Low energy sites are preferably filled first. With BIOVIA Amorphous Cell equilibrated disordered structure can be obtained. A number of tasks can be performed using BIOVIA Material Studio Amorphous Cell which are as follows-

1. General Modeling

2. Energy Options
3. Construction task
4. Packing task
5. Confined layer task

LAMMPS data file for simulation of nanocomposite can be easily exported by using msi2lmp executable file of LAMMPS.

4.3 LAMMPS (Large-scale Atomic/Molecular Massively Parallel Simulator)

4.3.1 Background

LAMMPS is a classical molecular dynamics program developed at Sandia National Laboratories, under United States Department of Energy. It is an open source code distributed under general public license. It is available at http://lammps.sandia.gov. The following section describes the feature of LAMMPS.

4.3.2 General features

The general features of LAMMPS are as follows:

i. Uses single as well as parallel processors.

ii. Message-passing parallelism (MPI).

iii. Simulation domain can be spatially decomposed for parallelism.

iv. Optional libraries : single-processor FFT and MPI.

v. Input script is used for running.

vi. Variables and formulas can be defined using syntax.

vii. Syntax for breaking out of loops and looping over runs.

4.3.3 Basic Structure of LAMMPS Program

Basic requirements of program in LAMMPS are discussed below-

4.3.3.1 Force fields

Some force fields used in LAMMPS are as follows:

i. Pairwise potentials: Buckhingam, Lennard-Jones, Morse, Born-Mayer-Huggins, soft, Yukawa, hydrogen bond, class 2 (COMPASS [34]).

ii. Charged pairwise potentials: Point-dipole, Coulombic.

iii. Many body potentials: EAM, modified EAM , Finnis/Sinclair EAM.

4.3.3.2 Atoms creation

The various methods of atom creation are-

i. read_data – this command is used to read the initial coordinates of atoms from a zipped text file or an ASCII text.
ii. lattice – this command is used to create atoms, inside the simulation box in the lattice points.
iii. delete_atoms – this command deletes atoms to create void.
iv. displace_atoms – randomizes atoms on a lattice initially or moves atoms to a large distance before a simulation.

4.3.3.3 Ensemble, boundary conditions and constraints

In LAMMPS ‘fix’ is any operation that is applied to the system during time stepping or minimization. For example, the updating of atom positions and velocities due to time integration, controlling temperature, applying constraint forces to atoms, enforcing boundary conditions, and computing diagnostics etc. Fixes perform their operations at different stages of the time step. If two or more fixes operate at the same stage of the time step, they are invoked in the order they were specified in the input script.

4.3.3.4 Boundary conditions

The boundary conditions employed in LAMMPS are:

a) p p p

b) p f p

c) p p s

Where ‘p’ represents periodic boundary conditions along the three directions, ‘f’ is for fixed and ‘s’ stands shrink wrapped. 'f' and 's' are non-periodic boundary conditions.

4.3.3.5 Integrator

The integrators available in LAMMPS are:

i. Velocity-Verlet integrator

ii. Rigid body integration

iii. Brownian dynamics

iv. Energy minimization via steepest descent or conjugate relaxation.

4.3.3.6 Energy Minimization

Energy minimization of the system is performed by LAMMPS by adjusting atom coordinates iteratively. There should be some stopping criteria to terminate the iterations. The system will have local minimum potential energy at that point. The 'min_style' command is used to set minimization algorithm. The distance atoms move in single iterations is bounded by the minimizers so that it is possible to push the atoms off and relax systems with large energies.

4.3.3.7 LAMMPS input script

LAMMPS executes program from an input script by reading commands, one line at a time. LAMMPS exits as the input script ends. LAMMPS takes action according to each command. It may read a file, set an internal variable, or run a simulation. Most commands can be changed as per the requirements. LAMMPS input generally has four parts:

i. Initialization

ii. Atom definition

iii. Settings

iv. Run a Simulation

4.4 OVITO

OVITO stands for Open Visualization Tool. It is a visualization software which is freely available online and is very useful in analyzing the simulation data iteratively. OVITO works on the principle of processing pipeline to visualize the various states of program. With the help of this software you can inspect particles individually. It runs on all major platforms including Mac OS, Microsoft Windows and Linux.

4.5 Modeling of Defects

The modeling of defects was done using Virtual Nanolab 2016.3. The steps required to generate the defects in CNTs are as follows-

4.5.1 Vacancy Defect

Vacancy defect can be easily created by using Crystal Builder tool in VNL. First, build a CNT of required chirality and length. Then select the vacant sites using random generator of MATLAB. Then, select those atoms from the co-ordinate list and delete them. After the defects have been created, optimize the structure using suitable force field and number of steps.

4.5.2 Stone-Wales Defect

To generate SW defect an add-on named tube wrapper needs to be installed first. Thereafter, build a graphene sheet of required length and chirality. Select the bond to be changed by using random generator of MATLAB. Rotate the bond by 90°. A 5-7-7-5 ring as shown in Fig. 4.1 has been generated. Then, use tube wrapper to revolve the graphene sheet about its axis and convert it into a nanotube. The geometry needs to be optimized and after that you can export the atom co-ordinates to LAMMPS data file format.

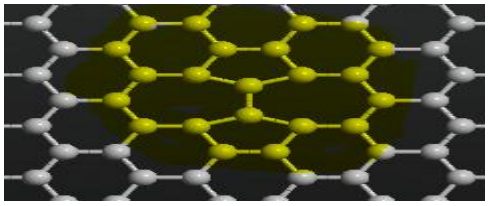

Fig. 4.1 Computer constructed model of SW defect.

4.6 Atomistic Model of CNT

Single-walled CNT with chirality of (9,0) and (18,0) of radii 3.525 and 7.051 Å, respectively was considered in this simulation. The length of CNTs is 75 Å approximately. The CNTs in this study are fixed at both the ends. The bullet is made of diamond having dimensions 35.67×35.67×7.13 $\mathring{A}^3$. The velocity of bullet varies between 100 m/s to 1100 m/s. The bullet is made to strike the nanotube at different heights and from a distance of 15Å from the axis of the nanotube. The dimension of bullet is chosen in such a manner that its width is greater than the maximum radius of nanotube after flattening, just like real conditions. The study has been conducted using Molecular Dynamics (MD) Simulation. In this study, defective CNTs are used for investigations. Defects are induced in the CNT with the help of VIRTUAL NANOLAB. This study is mainly concentrated on vacancy and SW defect. 1, 3, 5 and 10 numbers of defects were generated at random locations obtained from the random-generator command of MATLAB. Tersoff-Brenner [36] potential has been used to define the interatomic interactions and simulate deformations of CNT (See Appendix A). Fig. 4.2 depicts CNT before impact.

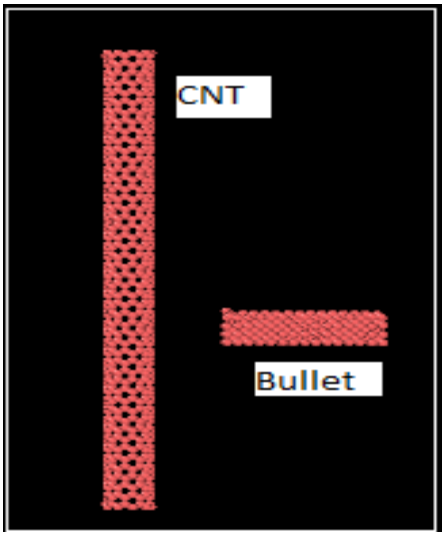

Fig.4.2 Initial MD model of CNT fixed at both ends.

4.7 Modeling of CNT Nanocomposite

Packing of epoxy around CNT was done by using BIOVIA Material Studio 8.0 Amorphous Cell is used. Dimensions of lattice are 40.28×40.28×62 $\mathring{A}^3$ with CNT of chirality (10,10). The length of CNT is same as the height of the lattice i.e., 62A^o . Density of polymer is 1 g/cm^3 and charges are assigned according Gatseiger methodology. First of all, CNT is modeled. Thereafter, polymeric chain of Epon 862 is modeled and packed around the CNT. After packing, the nanocomposite is optimized geometrically. Fig. 4.3 shows the monomer of Epon 862 molecule and Fig. 4.4 shows computer constructed model of Epon 862 molecule. Fig. 4.5 depicts finally packed structure of nanocomposite.

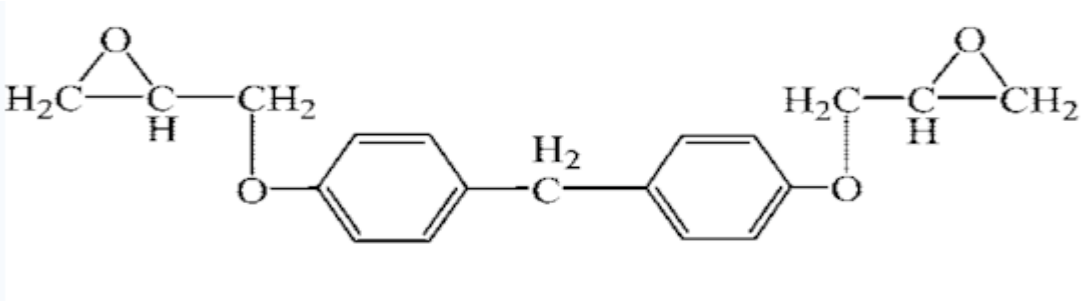

Fig. 4.3 Epon 862 monomer.

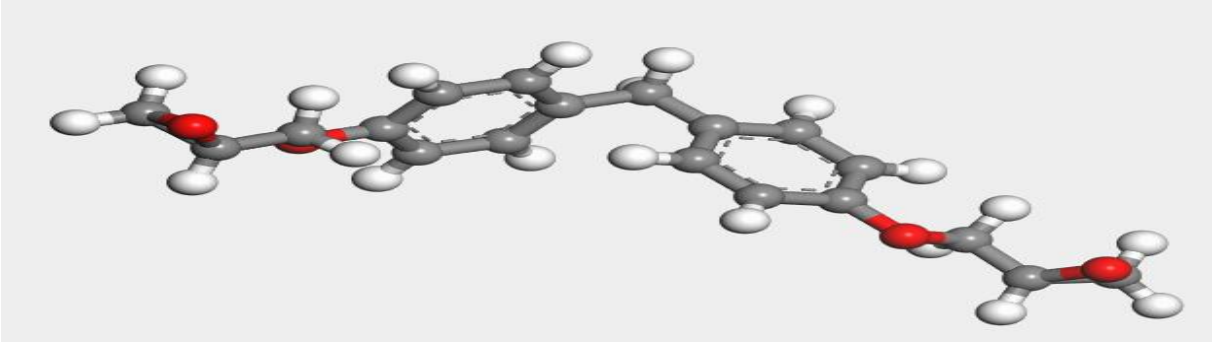

Fig. 4.4 Computer constructed molecules of Epon 862.

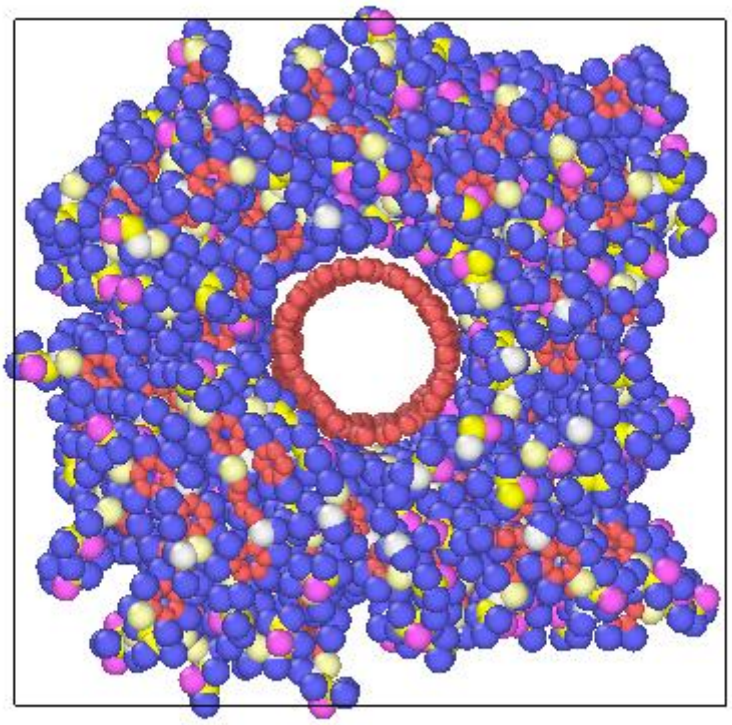

Fig. 4.5 Computer constructed Epon-862 matrix with CNT embedded in it (top view).

4.8 Atomistic Model of CNT-Nanocomposite

The Simulation model consists of Epon 862 matrix reinforced by long single walled CNTs. Dimensions of model are 40.28×40.28×62.0 A^o. Modeling has been done using Material Studio 8.0 . LAMMPS is used for simulation. The diamond bullet strikes the nanocomposites at different heights and velocities. Two opposite edges of nanocomposites are fixed. PCFF [35] potential is used to define the interactions between atoms of CNT and molecules of polymer. The structure exported from Material Studio needs to be minimized and equilibrated using LAMMPS program. The bullet dimensions is 15.0×10.0×5.0 $\acute{A}^3$ (See Appendix 2). The steps to be followed to optimize the structure are given below -

1. First of all, nanocomposite is minimized for 10,000 iterations to bring the polymer to equilibrated state. Thereafter, NVE ensemble is applied on the polymer to assign

velocities to particles. Langevin thermostat is also applied along with NVE to perform Brownian Dynamics on the particles interacting with each other.

2. Thereafter, polymers are allowed to deform to attain its original dimensions. NVT ensemble is applied for 30,000 steps and the structure thus obtained is minimized for 10,000 time steps. Deformations are usually performed in more than one steps so that atoms are not lost in the simulation procedure.
3. Next step includes annealing of nanocomposite to a temperature of 600 K using NVT. thermostat. The model is then quenched back to 300 K by applying NVT ensemble.
4. NPT thermostat is applied to upgrade positions, velocities, orientation and angular velocity of particles. The thermostat is applied at 300 K temperature. Nanocomposite regains its original shape. It can now be used for further simulation. Fig. 4.6 shows undeformed model of nanocomposite.

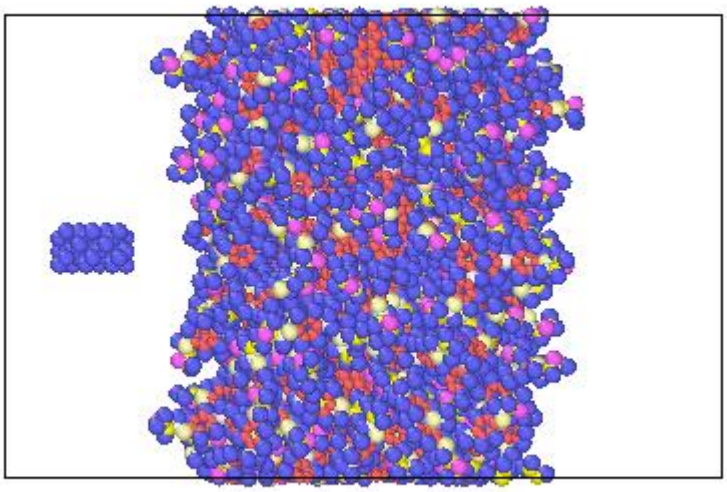

Fig. 4.6 Computer constructed nanocomposite model with bullet (before impact).

Chapter-5

Results and Discussions

5.1 Validation Study

The results of CNT were validated by a previous study [16]. When the diamond bullet with dimension 35.67×35.67×7.13 $Å^3$ strikes at different heights, energy is absorbed by CNT. Results obtained from present simulation are quite in agreement with the study. Energy absorbed increases with increase in speed. CNT model breaks if the velocity of bullet is greater than 1500 m/s. Absorbed energy is maximum when the bullet strikes in the middle. In the paper, energy is calculated at different combinations of bullet speeds and heights. The graph in Fig. 5.1 shows bullet speeds used to strike CNT at different heights. Comparison of two studies is shown in Fig. 5.2 and results are quite in agreement with the previous ones.

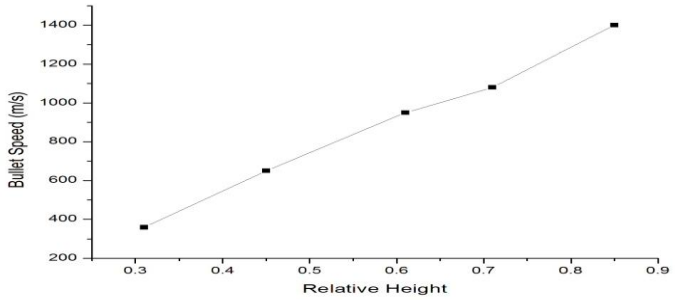

Fig. 5.1 Variation of bullet speed relative to height

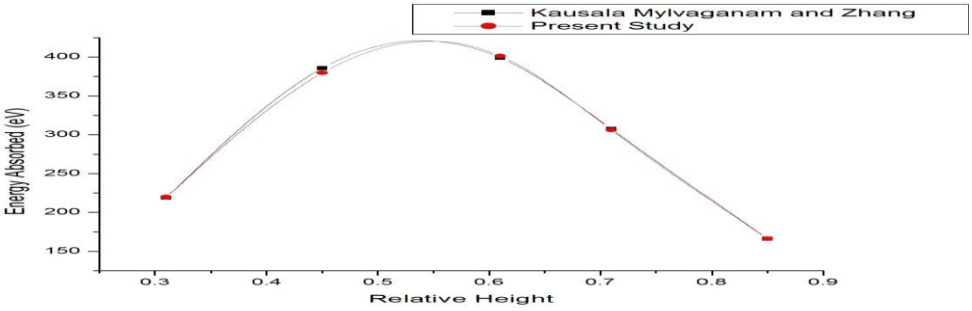

Fig. 5.2 Maximum energy absorbed by bullet when the bullet strikes (9,0) CNT at different relative heights

5.2 Results and Discussions

In the ballistic impact study of CNT, bullet with velocities 360m/s, 650 m/s and 1050 m/s strikes it at relative heights of 0.5 and 0.71. When the bullet strikes CNT, it bends elastically to a certain limit and then gets detached from one of the ends. Energy absorbed is calculated when the carbon bonds break and CNT gets detached. The deformation of CNT fixed at both ends when the bullet strikes it is shown in Fig. 5.3.

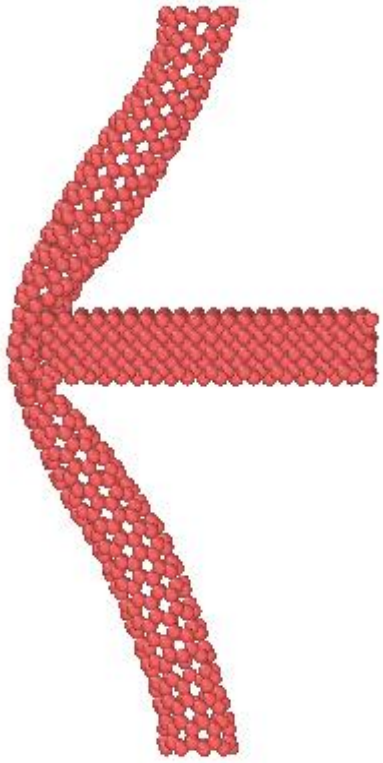

Fig. 5.3 Deformed model of (9,0) CNT fixed at both ends.

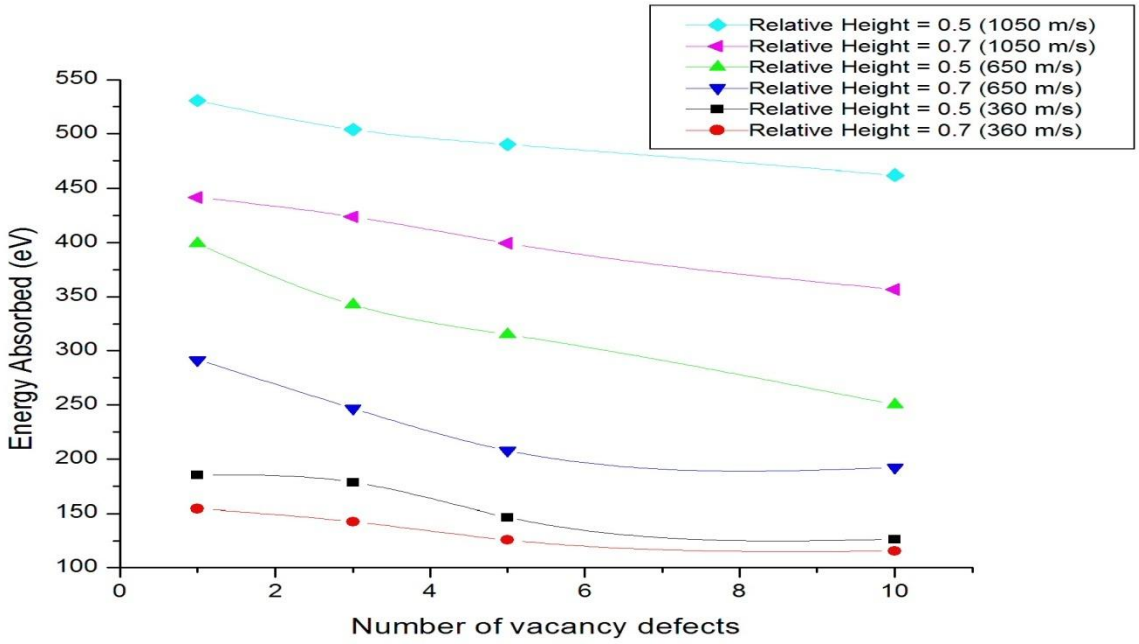

Fig. 5.4 Variation of maximum absorption energy with the number of vacancy defects in (9,0) CNTs fixed at both ends and the bullet velocity.

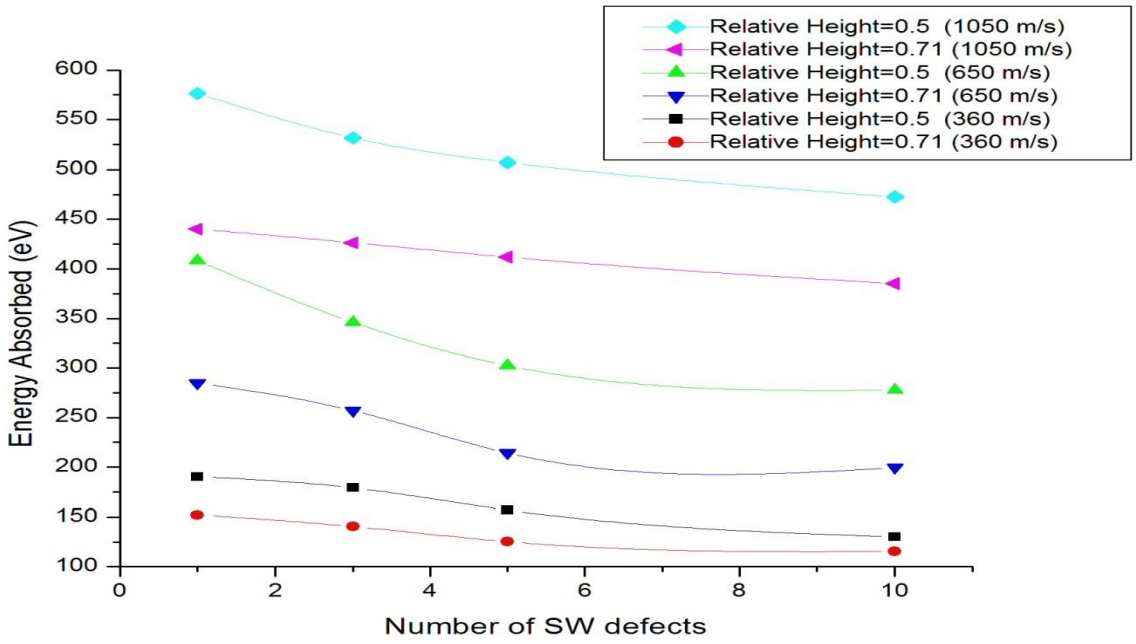

Fig. 5.5 Variation of maximum absorption energy with the number of SW defects in (9,0) CNTs fixed at both ends and the bullet velocity.

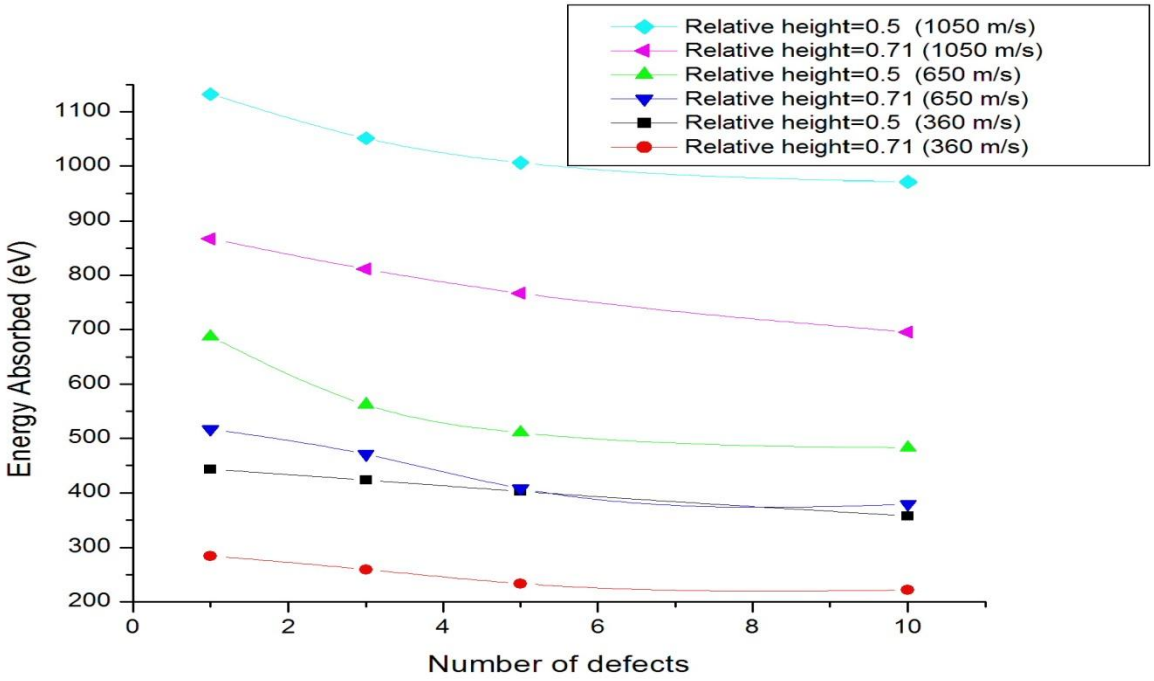

Fig. 5.6 Variation of maximum absorption energy with the number of vacancy defects in (18,0) CNTs fixed at both ends for different bullet velocities.

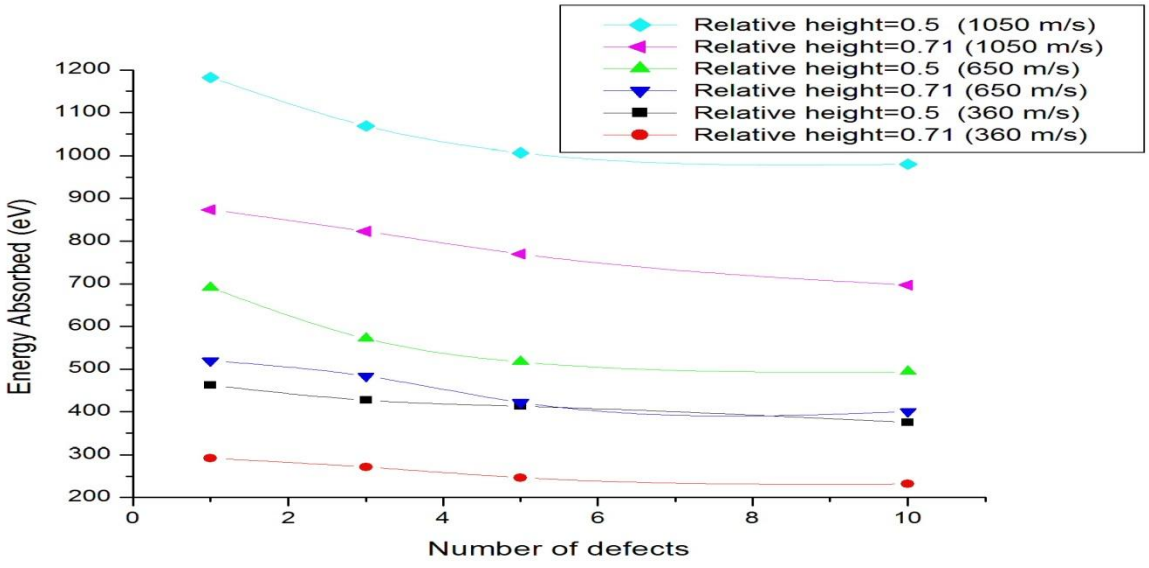

Fig. 5.7 Variation of maximum absorption energy with the number of SW defect in (18,0) CNTs fixed at both ends for different bullet velocities.

Fig. 5.4 shows the variation of maximum energy absorbed by (9,0) with no. of vacancy defects. It can be observed from Fig. 5.4 that when bullet strikes CNT at mid-point, energy absorbed is the highest and it is decreased when the bullet strikes at positions nearer to the fixed ends. Also, the energy absorbing capacity increases with the increase in the velocity of the bullet. The same can be observed from Fig. 5.5 drawn for the case of SW-defects. From Figs. 5.6 and 5.7, it can be concluded that energy absorption also depends on the radius of CNT, i.e., (18,0) CNT absorbs more energy than (9,0) CNTs. Figs. 5.4-5.7 also show that energy absorbed by CNTs with 1 and 3 defects (for vacancy and SW both) is almost same, and it decreases with increase in the number of defects. Also, CNTs with SW defects show lesser degradation in energy absorbing capacity as compared to CNTs with vacancy defects, irrespective of the chirality of the CNT.

Fig. 5.8 shows the variations of energy absorbed by nanocomposite when the bullet strikes at different heights with different velocities. When bullet strikes nearer to the ends energy absorbing capacity is less. Further, the absorbed energy increases with increase in velocity. From Fig. 5.8, it can also be observed that when we use CNT-nanocomposite absorbed energy increases significantly as compared to CNT only. The CNT inside nanocomposite breaks as bullet passes through it. Fig. 5.9 shows the deformed state of nanomposite.

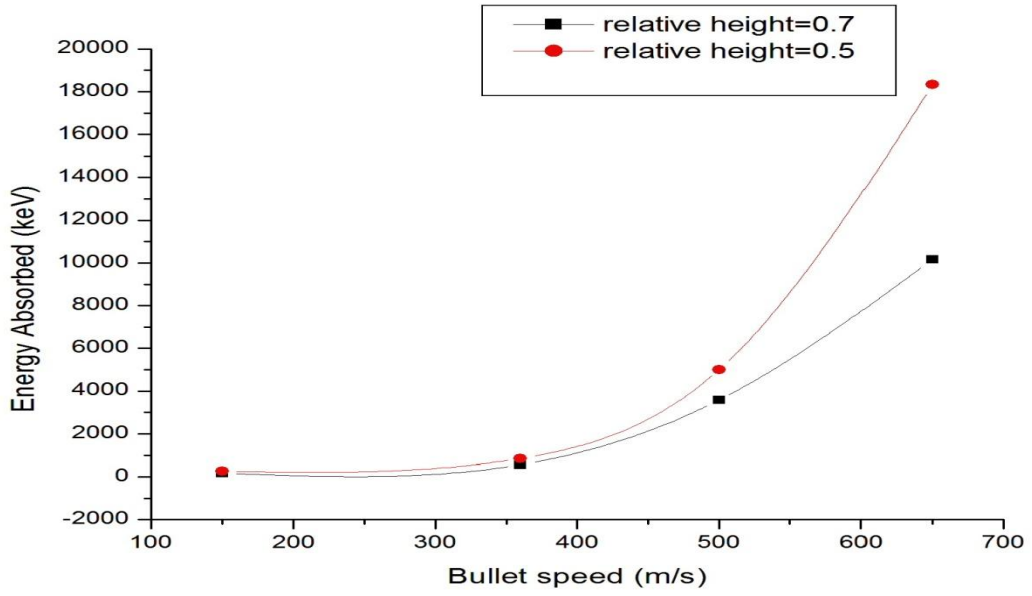

Fig. 5.8 Variation of maximum absorption energy with the bullet speed and the relative height at which bullet strikes nanocomposite.

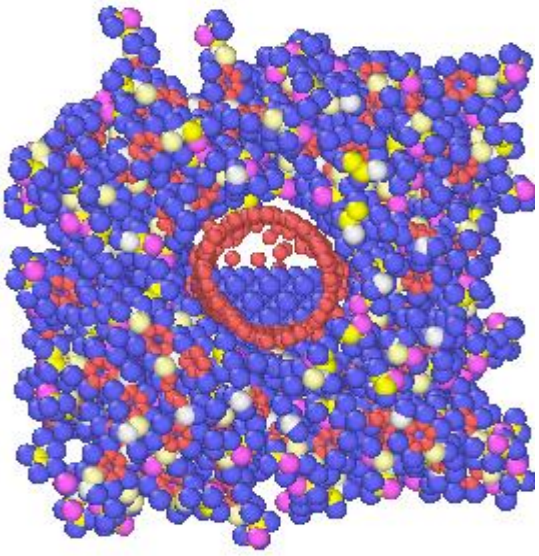

Fig. 5.9 Deformation of nanocomposite when the bullet strikes at the mid-point.

Chapter-6

Conclusions and Future Scope

6.1 Conclusions

. A Molecular Dynamics (MD) study has been conducted to investigate the potential applications of CNTs and CNT-nanocomposite in mitigating ballistic impacts. Two types of defects namely vacancy and SW defect were induced in CNTs of different diameters to examine their effect of energy absorbing capacity of CNTs. Also, CNT was used as reinforcement in epoxy matrix and energy absorbing capacity was calculated. Modeling was done with using VNL (for defective CNTs) and Material Studio (for nanocomposite). Tersoff potential was used for CNT and PCFF for nanocomposite. LAMMPS program was used for simulation and OVITO was used for visualization. A bullet made up of diamond having flat surface was allowed to strike CNTs and nanocomposites. The velocity of bullet was varied. The effect of striking bullet at different heights was also studied.

From the simulations done so far it is concluded that defective CNTs have lower energy absorbing capacity under ballistic impact. The bullet striking at mid-point and with high velocity is found to have maximum energy absorbing capacity. CNTs with SW defects show comparatively lesser degradation in absorbed energy as compared to CNTs with vacancy defects. CNTs cannot sustain bullets higher than 1500 m/s. The temperature also rises at the point of maximum deformation. Rise in temperature for lower velocity is about 30-40 K and it reaches to 100-200 K for higher velocities. As epoxy polymer is reinforced with CNTs the energy absorption increases by a factor of 1000. The absorbed energy decreases as the bullet strikes the CNT and the bonds break. CNT based nanocomposites are very promising in absorbing high energies under blasts.

6.2 Future Scope

- Energy absorbing capacity of CNTs with defects like pertubation and doping can also be considered.
- Mechanical behavior of nanocomposites reinforced with defective CNTs under blast have not been discussed.
- Variation in maximum absorbed energy if curing agents like DETA with epoxy polymer are used to increase its strength can also be considered.
- Ballistic impact on nanocomposite when the interface properties are also considered.
- Maximum energy absorbed by other promising materials such as graphene can also be studied.
- Cross linking of polymer chains can also be considered while studying ballistic impact of nanocomposite.

Appendix-A

Simulation procedure-

LAMMPS program is to study the ballistic impact on CNTs.

I. Initialization Section

```
units           metal
boundary        p p p
atom_style      atomic
neighbor        0.01 nsq
```

II. Atom Definition Section

For CNT

```
region          box block -40.0 65.0 -10.0 40.0 -5 110.0 units box
create_box      2 box
mass            1 12.010700
```

For Diamond bullet

```
mass            2 12.010700
lattice         diamond 3.57
region          diamond block 20 55.67 4.3140155 39.9840155 56.25 63.38 units box
create_atoms    1 region diamond units box
```

III. Add CNT data file

```
read_data "C:\Users\Administrator\Desktop\lammps\cntdata.data" add append
```

IV. Settings section

```
pair_style      airebo 3.0 0 0                    (interatomic potential)
```

```
pair_coeff      * * C:\Users\Administrator\Desktop\lammps\CH.airebo C C
min_style cg                                                    (minimization)
minimize 1.0e-5 1.0e-5 100000 10000
```

V. Regions & groups

```
region  lower block INF INF INF INF INF 3 units box
region  upper block INF INF INF INF 78 INF units box

group   upper region upper
group   lower region lower
group   boundary union upper lower
```

VI. Fixes

```
fix         1 boundary setforce 0.0 0.0 0.0
fix         2 cnt nve
fix         3 cnt temp/berendsen 300.0 300.0 100.0
fix         4 indent move linear -3.6 0.0 0.0
```

VII. Compute

```
Compute     tem all temp                    (Compute temperature)
compute     keratom all ke/atom             (Kinetic energy of all atoms)
compute     ke all reduce sum c_keratom
compute     kecnt cnt reduce sum c_keratom  ( Kinetic energy of CNT)
```

VIII. Run a simulation

```
Run         6000
```

Output

The LAMMPS program gives following output files-

1. Dump File (.lammpstrj)- This file contains the co-ordinates of atoms of the final structure obtained after simulation. It is also useful for studying deformation.

2. Log file- This file contains thermodynamic data e.g pressure, temperature, volume, and total energy after a particular timestep.

3. Log.lammps file.

Appendix-B

Simulation procedure-

LAMMPS program is to study the ballistic impact on nanocomposite-

I. Atom Definition Section

Define the path of nanocomposite file

read_restart "C:\Users\Administrator\Desktop\epoxyy\restart\9.2.restart"

change_box all y final -25.358048192 70.684076246 boundary p p p set units box

group CNT type 1

group polymer type 2 3 4 5 6

II. Initialization Section

echo screen

lattice diamond 3.57

region diamond block 12.5 27.5 55.0 65.0 28.5 33.5 units box

create_atoms 2 region diamond units box

mass 2 12.010700

group indent region diamond

timestep 0.002

III. Regions &groups

variable lo equal zlo+3.5

variable hi equal zhi-3.5

```
region  lower block INF INF INF INF INF ${lo} units box
region  upper block INF INF INF INF ${hi} INF units box

group   upper region upper
group   lower region lower
group   boundary union upper lower
group   poly subtract all boundary indent
```

IV. Fixes

```
fix         1 all nve
fix         2  boundary setforce 0.0 0.0 0.0
fix         3 all temp/rescale 100 0.1 0.1 0.01 1.0
fix         4 indent move linear 0.0 -5.0 0.0
```

V. Results

```
compute         peratom all pe/atom
compute         pe all reduce sum c_peratom
compute         pepoly poly reduce sum c_peratom
compute         keratom all ke/atom
compute         ke all reduce sum c_keratom
compute         kepoly poly reduce sum c_keratom
compute         tem all temp
compute         mytemp poly temp
#run with indenter
```

```
thermo 10
thermo_style custom step temp  etotal press pe c_pepoly ke c_kepoly c_mytemp
dump dump1 all atom 100 C:\Users\Administrator\Desktop\epoxyy\ncntbound360d1.lammpstrj
run          3000
```

References

[1] H. W. Kroto, J. R. Heath, S. C. O'Brien, R. F. Curl, and R. E. Smalley, "C 60: buckminsterfullerene," *Nature*, vol. 318, pp. 162–163, 1985.

[2] S. C. Baker, D. P. Kelly, and J. C. Murrel, "© 19 9 1 Nature Publishing Group," *Nature*, vol. 350, pp. 627–628, 1991.

[3] C. E. Baddour and C. Briens, "Carbon nanotube synthesis: a review," *Int. J. Chem. React. Eng.*, vol. 3, no. 1, 2005.

[4] M. S. Dresselhaus and G. Dresselhaus, "Phaedon Avouris, eds. 2001. Carbon nanotubes: synthesis, structure, properties, and applications." Berlin: Springer Publishers.

[5] S. Reich, C. Thomsen, and J. Maultzsch, *Carbon nanotubes: basic concepts and physical properties*. John Wiley & Sons, 2008.

[6] S. V Rotkin and S. Subramoney, *Applied physics of carbon nanotubes: fundamentals of theory, optics and transport devices*. Springer Science & Business Media, 2006.

[7] T. Belin and F. Epron, "Characterization methods of carbon nanotubes: a review," *Mater. Sci. Eng. B*, vol. 119, no. 2, pp. 105–118, 2005.

[8] N. V. David, X.-L. Gao, and J. Q. Zheng, "Ballistic Resistant Body Armor: Contemporary and Prospective Materials and Related Protection Mechanisms," *Appl. Mech. Rev.*, vol. 62, no. 5, p. 50802, 2009.

[9] S. C. Tjong, *Carbon nanotube reinforced composites: metal and ceramic matrices*. John Wiley & Sons, 2009.

[10] E. Pop, D. Mann, Q. Wang, K. Goodson, and H. J. Dai, "Thermal conductance of an individual single-wall carbon nanotube above room temperature," *Nano Lett.*, vol. 6, no. 1, pp. 96–100, 2006.

[11] P. Szweda and P. Szweda, "World â€^{TM} s largest Science , Technology & Medicine Open Access book publisher Antimicrobial Activity of Honey Antimicrobial Activity of Honey."

[12] P. Avouris, “Molecular Electronics with Carbon Nanotubes,” *ChemInform*, vol. 34, no. 8, pp. 1026–1034, 2003.

[13] A. Krishnan, E. Dujardin, T. W. Ebbesen, P. N. Yianilos, and M. M. J. Treacy, “Young’s modulus of single-walled nanotubes,” *Phys. Rev. B*, vol. 58, no. 20, pp. 14013–14019, 1998.

[14] A. B. Dalton, S. Collins, J. M. Razal, and V. Howard, “Super-tough carbon-nanotube fibres,” vol. 886, p. 2002, 2002.

[15] Y. Jin and F. G. Yuan, “Simulation of elastic properties of single-walled carbon nanotubes,” *Compos. Sci. Technol.*, vol. 63, no. 11, pp. 1507–1515, 2003.

[16] K. Mylvaganam and L. C. Zhang, “Energy absorption capacity of carbon nanotubes under ballistic impact,” no. April, pp. 12–14, 2006.

[17] K. Mylvaganam and L. C. Zhang, “Ballistic resistance capacity of carbon nanotubes,” *Nanotechnology*, vol. 18, no. 47, p. 475701, 2007.

[18] U. A. Joshi, S. C. Sharma, and S. P. Harsha, “Characterizing the strength and elasticity deviation in defective CNT reinforced composites,” *Compos. Commun.*, vol. 2, no. June, pp. 9–14, 2016.

[19] O. Lourie, D. Cox, and H. Wagner, “Buckling and Collapse of Embedded Carbon Nanotubes,” *Phys. Rev. Lett.*, vol. 81, no. 8, pp. 1638–1641, 1998.

[20] “chopra1995.pdf.” .

[21] W. Qian, F. Wei, T. Liu, Z. Wang, and Y. Li, “What causes the carbon nanotubes collapse in a chemical vapor deposition process,” *J. Chem. Phys.*, vol. 118, no. 2, pp. 878–882, 2003.

[22] W. Qian *et al.*, “The evaluation of the gross defects of carbon nanotubes in a continuous CVD process,” *Carbon N. Y.*, vol. 41, no. 13, pp. 2613–2617, 2003.

[23] Y. Ye, H. Chen, J. Wu, and L. Ye, “High impact strength epoxy nanocomposites with natural nanotubes,” vol. 48, pp. 6426–6433, 2007.

[24] G. S. Langdon, “SCIENCE AND Failure characterisation of blast-loaded fibre – metal laminate panels based on aluminium and glass – fibre reinforced polypropylene,” vol. 67, pp. 1385–1405, 2007.

[25] K. Iqbal, S. Khan, A. Munir, and J. Kim, “Impact damage resistance of CFRP with nanoclay-filled epoxy matrix,” *Compos. Sci. Technol.*, vol. 69, no. 11–12, pp. 1949–1957, 2009.

[26] M. M. Reda, A. B. Colak-altunc, and M. Al-haik, “Composites : Part B A multi-objective optimization approach for design of blast-resistant composite laminates using carbon nanotubes,” *Compos. Part B*, vol. 40, no. 6, pp. 522–529, 2009.

[27] M. R. Ayatollahi, “ch ive,” vol. c, no. 10, pp. 835–843, 2011.

[28] J. A. King, D. R. Klimek, I. Miskioglu, and G. M. Odegard, “Mechanical properties of graphene nanoplatelet / epoxy composites,” 2014.

[29] I. Taraghi, A. Fereidoon, and F. Taheri-behrooz, “Low-velocity impact response of woven Kevlar / epoxy laminated composites reinforced with multi-walled carbon nanotubes at ambient and low temperatures,” *J. Mater.*, vol. 53, pp. 152–158, 2014.

[30] E. T. Thostenson, Z. Ren, and T.-W. Chou, “Advances in the science and technology of carbon nanotubes and their composites: a review,” *Compos. Sci. Technol.*, vol. 61, no. 13, pp. 1899–1912, 2001.

[31] R. Zhu, E. Pan, and A. K. Roy, “Molecular dynamics study of the stress-strain behavior of carbon-nanotube reinforced Epon 862 composites,” *Mater. Sci. Eng. A*, vol. 447, no. 1–2, pp. 51–57, 2007.

[32] P. K. R. A. V. U. S. Chaudhary, “Effect of SBA-15 on the energy absorption characteristics of epoxy resin for blast mitigation applications,” pp. 709–719, 2013.

[33] M. Grujicic, B. P. D. C. Angstadt, K. L. Koudela, A. R. L. Building, and B. A. Cheeseman, “Ballistic-Performance Optimization of A Hybrid Carbon-Nanotube / E-Glass Reinforced Poly-Vinyl-Ester-Epoxy-Matrix Composite Armor The material model for a Multi-Walled Carbon Nanotube (MWCNT) reinforced,” *J. Mater. Sci.*, vol. 42, no. 14, pp. 5347–5359, 2007.

[34] H. Sun, “COMPASS: An ab Initio Force-Field Optimized for Condensed-Phase ApplicationsOverview with Details on Alkane and Benzene Compounds,” *J. Phys. Chem. B*, vol. 102, no. 38, pp. 7338–7364, 1998.

[35] H. Sun, S. J. Mumby, J. R. Maple, and A. T. Hagler, “An ab Initio CFF93 All-Atom Force Field for

Polycarbonates," *J. Am. Chem. Soc.*, vol. 116, no. 7, pp. 2978–2987, 1994.